Available online at www.sciencedirect.com
SCIENCE DIRECT
Catalysis Today 116 (2006) 226–233
CATALYSIS TODAY
www.elsevier.com/locate/cattod

Hydrocarbon oxidation and aldol condensation over basic zeolite catalysts

Junhui Li, Jianren Tai, Robert J. Davis *

Department of Chemical Engineering, University of Virginia, Charlottesville, VA 22904-4741, USA

Available online 30 May 2006

Abstract

Ion-exchanged X zeolites, with and without occluded cesium, were tested as catalysts for hydrocarbon oxidation and aldol condensation. Infrared spectroscopy confirmed that combustion products were formed during the oxidation reactions. The reaction profile of 1-butene or butane oxidation over zeolite X in the range of 473–523 K revealed an induction time followed by a maximum in CO_2 production. Ion-exchanged NaX and CsX exhibited a higher maximum CO_2 production rate than MgX during butene oxidation at 473 K. Addition of Cs to CsX above ion-exchange capacity decreased the CO_2 production rate, indicating that basicity was not important for the reaction. Silica, alumina and Cs-doped alumina were several orders of magnitude less active than NaX and CsX for 1-butene oxidation at 523 K. In general, the oxidation of butane was slower than that of 1-butene. The high electric field associated with cations in the zeolite pores is suggested to be important for the oxidation reactions. In contrast to hydrocarbon oxidation, the condensation reaction of propionic acid and formaldehyde to form methacrylic acid at 598 K depended on the basicity of the zeolite, with the activity increasing in the order NaX < KX < CsX. Increasing the basicity of CsX by occluding Cs in the pores beyond ion-exchange capacity further increased the activity.

Keywords: Zeolite; Hydrocarbon oxidation; Infrared spectroscopy; Propionic acid; Formaldehyde; Methacrylic acid

1. Introduction

Ion-exchanged faujasites such as zeolites X and Y are microporous aluminosilicates with unique properties in oxidation catalysis as well as acid–base base catalysis. For example, hydrocarbon oxidation reactions induced by photons within zeolite structures have been extensively studied over recent years. Researchers have achieved oxidation of ethane, propane, isobutene and 1-butene with high selectivity under irradiation with visible light as well as under dark thermal conditions in cation-exchanged zeolites, such as NaY, CaY, SrY, and BaY [1–3]. A proposed mechanism by Frei and coworkers in Expression (1) involves a radical cation and O_2^- by activating dioxygen and hydrocarbon with electron transfer from the hydrocarbon to the oxygen molecule. The produced hydrocarbon radical cations have strong acidity and therefore readily donate the proton (H^+) to $^-O_2^\bullet$ to yield $R^\bullet$ (alkyl or allyl) and $HOO^\bullet$ [1,2,4].

$$RH + O_2 \underset{\Delta T(h\nu)}{\longrightarrow} RH^{\bullet +} + {}^-O_2^\bullet \rightarrow R^\bullet + HOO^\bullet \quad (1)$$

Charge-transfer from hydrocarbon to dioxygen can be induced by absorption of a photon by a hydrocarbon-O_2 collisional complex, or happens spontaneously in a thermal process if molecules were occluded in a highly ionic environment.

Ultraviolet (UV) light-induced formation of hydrocarbon-O_2 charge-transfer states was reported early by Tsubomura and Mulliken [5]. The more recent studies by Frei and coworkers observed that the high electrical field inside the supercage of dehydrated alkali or alkaline-earth zeolite Y (NaY 0.3 V Å^{-1}, BaY 0.9 V Å^{-1}) caused a large red shift of hydrocarbon-O_2 charge-transfer transitions from the UV into the visible range [4,6], indicating a strong stabilization of the excited charge-transfer state by the zeolite cage. Researchers proposed that the strong stabilization of a hydrocarbon RH^+–O_2^- charge-transfer pair inside a zeolite cage is due to the interaction of its large dipole with the high electrostatic field near alkali or alkaline earth cations [7]. Interestingly, the dark thermal oxidation of hydrocarbons was catalyzed by zeolites X and Y at low temperature (353 K) [1,2,6], and those reactions were assumed to proceed via the same mechanism as the photoassisted oxidation, i.e. electron transfer involving the superoxide anion radical [2]. Vanoppen et al. found that activity decreased in the order CaY > SrY > BaY > NaY during cyclohexane auto-oxidation, which provided further evidence that the electrostatic

* Corresponding author.
E-mail address: rjd4f@virginia.edu (R.J. Davis).

0920-5861/$ – see front matter © 2006 Elsevier B.V. All rights reserved.
doi:10.1016/j.cattod.2006.01.032

field plays an important role in determining the extent of hydrocarbon oxidation in zeolites [8].

In addition to oxidation catalysis, alkali metal ion-exchanged zeolite X is a solid base which catalyzes reactions such as side-chain alkylation of toluene with methanol to form styrene and ethylbenzene [9]. Stronger base catalysts are formed when alkali metal compounds are occluded in the zeolite micropores and activated by thermal treatment. For example, 1-butene double bond isomerization is catalyzed by occluded cesium oxycarbonate in zeolite X [10].

In this paper, ion-exchanged zeolite X samples, with and without occluded alkali metal compounds, were explored as hydrocarbon oxidation catalysts and as base catalysts for the condensation of propionic acid with formaldehyde.

2. Experimental methods

2.1. Catalyst preparation

A commercial sample of NaX (Union Carbide, lot no. 07483-36) was triply ion-exchanged with 1 M aqueous solutions of sodium acetate, potassium nitrate or cesium acetate (Aldrich 99.9%) for 24 h at room temperature. Magnesium-exchanged zeolite Y was prepared by triply ion-exchanging NaY (Union Carbide, lot no. 943191060078) with 1 M aqueous solutions of magnesium acetate (Aldrich, 99%) for 24 h at room temperature, respectively. The resulting NaX, KX, CsX and MgY were washed with deionized distilled water (>1 L/g zeolite) and dried in air at 373 K overnight.

Zeolites containing excess alkali species (in addition to the ion-exchanged cations) were prepared by impregnation of the ion-exchanged zeolites with cesium acetate (Aldrich, 99.99%) solution. The concentrations of the cesium salts were determined by the desired Cs-loading and the amount of water the zeolite can absorb during the wet impregnation. The zeolites with occluded cesium were denoted as Cs/CsX. The impregnated catalysts were dried overnight in air at 373 K and calcined in flowing air at 773 K for 5 h.

A sample denoted as Cs/γ-Al_2O_3 was prepared in order to explore the effect of support structure on the supported cesium species. The γ-Al_2O_3 was obtained from Mager Scientific Inc. The Cs/γ-Al_2O_3 sample was prepared by incipient wetness impregnation of the alumina support with an aqueous solution of cesium acetate with appropriate concentration. The catalyst was dried in air at 373 K overnight and calcined in air for 5 h. Magnesia (Ube) and silica gel (Fisher, chromatographic grade) were also tested as catalysts.

A Cs/Bi/SiO_2 catalyst was synthesized via sol–gel method. Cesium acetate (Aldrich, 99.99%) was dissolved in distilled, deionized water, while bismuth chloride (Alfa Aesar, 99.99%) was dissolved in hydrochloric acid. The two solutions were then added to a colloidal silica solution (Dupont Ludox, 30 wt.% silica suspended in water) under stirring at room temperature until a hydrogel was formed. The hydrogel was left at room temperature overnight for aging then dried in air at 373 K. The resulting solid cake was crushed and calcined in air at 813 K for 8 h. The nominal composition of the catalyst is Cs (4 wt.%)/Bi (0.5 wt.%)/SiO_2.

2.2. FT-IR spectroscopy

Cesium-loaded zeolite was pressed into a self-supporting pellet and loaded into a transmission cell for IR spectroscopy. The sample was pretreated in flowing He (100 mL min^{-1}, 99.999%, BOC Gases, further purified with a Supelco OMI-2 indicating purifier), at 773 K for 5 h before cooling. A mixture of O_2 (50 mL min^{-1}) and 1-butene (5 mL min^{-1}) was co-fed to the in situ infrared cell. After about 60 min of reaction, a Pfieffer turbomolecular pump was used to evacuate the cell to 9.6×10^{-5} Torr while cooling. Absorbance spectra of the catalyst were averaged from 300 scans at 473 K collected on a Bio Rad FTS-60A spectrometer operating with a resolution of 2 cm^{-1}. A similar procedure was used for the study of butane oxidation on zeolites.

2.3. Hydrocarbon oxidation

The hydrocarbon oxidation was performed in a single pass, continuously fed fixed bed reactor containing about 0.3 g of zeolite catalyst. A sample was first pretreated in situ at 773 K for 300 min under flowing helium (BOC Gases, 99.999%, 35 mL min^{-1}). The total flow rate of the feed stream was approximately 43 mL min^{-1} with 9.3% 1-butene (Aldrich, 99+%) and 9.3% O_2 (BOC Gases, 99.999%) in helium. The reaction temperature range was between 473 and 573 K. Products from the reaction were analyzed online by an HP5890 II gas chromatograph equipped with a flame ionization detector (FID) and a thermal conductivity detector (TCD).

2.4. Aldol condensation

The aldol condensation reaction was carried out in a fixed bed flow reactor system at 598 K. The catalyst was supported on a quartz frit in a single pass quartz reactor. Trioxane (Aldrich, 99.9%) was dissolved in propionic acid, PA (Aldrich, 97%) and injected via a syringe pump at a rate of 0.4 mL h^{-1} into a 35 mL min^{-1} helium stream. The vaporized liquid and helium stream passed through a heating zone (700 K) to crack trioxane into formaldehyde, FA. The molar ratio of the reactants in the feed stream was He:PA:FA = 52:3:2. When needed, an appropriate amount of water was added to the reactant solution. The products were collected in liquid isopropyl alcohol at 273 K and analyzed by an HP 5890 gas chromatograph equipped with a 30 m HP Innowax capillary column and an FID detector. *N*-heptane was added to the product mixture as an internal standard.

3. Results and discussion

3.1. FT-IR spectroscopy after hydrocarbon oxidation

Fig. 1 shows the FT-IR spectra of CsX exposed to dioxygen and 1-butene, dioxygen and butane, 1-butene, butane, and

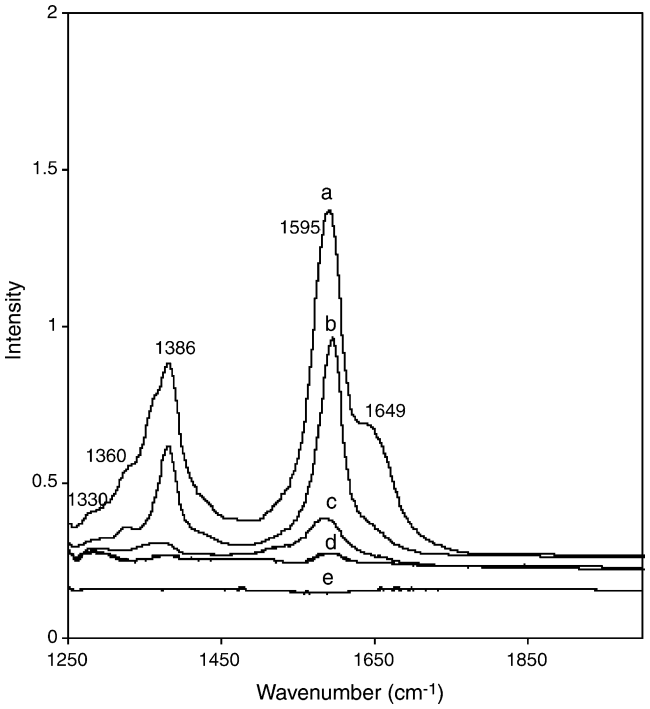

Fig. 1. Infrared spectra of CsX at 473 K after (a) pretreated at 773 K in flowing He for 5 h, exposed to 1-butene and dioxygen; (b) pretreated at 773 K in flowing He for 5 h, exposed to butane and dioxygen; (c) pretreated at 773 K in flowing He for 5 h, exposed to 1-butene; (d) pretreated at 773 K in flowing He for 5 h, exposed to butane; (e) pretreated at 773 K in flowing He for 5 h, exposed to O_2, then evacuated at 10^{-4} Torr for 30 min.

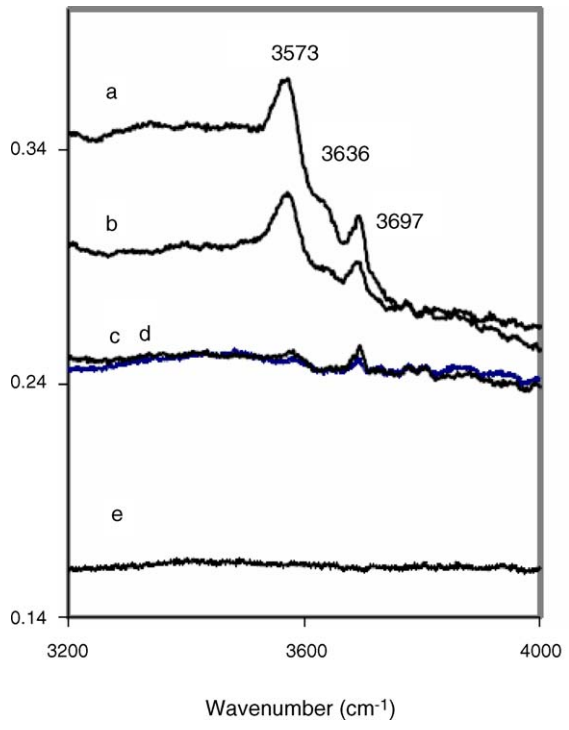

Fig. 2. Infrared spectra of the hydroxyl region of CsX at 473 K. The individual spectra are associated with pretreatments designated in Fig. 1.

dioxygen respectively after being pretreated at 773 K, then evacuated at 10^{-4} Torr for 30 min at 473 K. The FT-IR spectra of individual species of 1-butene, butane and dioxygen adsorption showed no apparent IR bands, which indicated the adsorption of these species on CsX was relatively weak. However, a strong band at 1595 cm^{-1} together with three bands at 1386, 1360 and 1338 cm^{-1} were observed when 1-butene and dioxygen were co-fed. These features reported in Fig. 1(a) and (b) might be due to the asymmetric and symmetric stretching modes of adsorbed CO_2 on CsX, respectively [11–13]. Earlier work in our lab revealed bands associated with surface carbonate at 1611 and 1347 cm^{-1} after adsorption of CO_2 on CsX and heating to 473 K [11]. However, Xu et al. report the asymmetric and symmetric bands of carboxylate ($RCOO^-$) in SrY at 1584 and 1367 cm^{-1} [14]. Therefore, the IR spectra of CsX after oxidation of butene are consistent with the presence of partial and/or total oxidation products in the zeolite pores.

The IR band at 1649 cm^{-1} observed in Fig. 1(a) and (b) likely arose from the adsorption of water on zeolite X. Beta et al. reported the vibrational frequency of HOH bending on hydrated zeolites at 1653 cm^{-1} [15]. Up to three bands of different intensities in the OH-stretching vibration region from 3000 to 3800 cm^{-1} were also observed (Fig. 2). The IR spectrum in the OH-stretching region for adsorption of four water molecules per unit cell of CsX is reported to have three peaks at 3572, 3639 and 3703 cm^{-1} [15]. All features associated with the OH stretching of adsorbed water on CsX are in good agreement with our experimental results, which

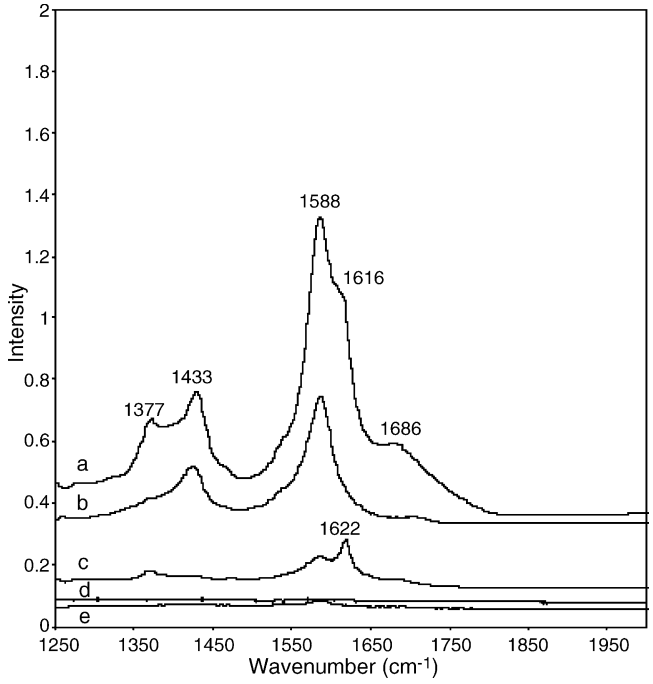

Fig. 3. Infrared spectra of NaX at 473 K after being (a) pretreated at 773 K in flowing He for 5 h, exposed to 1-butene and dioxygen; (b) pretreated at 773 K in flowing He for 5 h, exposed to butane and dioxygen; (c) pretreated at 773 K in flowing He for 5 h, exposed to 1-butene; (d) pretreated at 773 K in flowing He for 5 h, exposed to butane at 473 K; (e) pretreated at 773 K in flowing He for 5 h, exposed to O_2, then evacuated at 10^{-4} Torr for 30 min.

suggests that water is formed during the butene oxidation reaction. The fact we observed up to three bands in the OH-stretching region implied that they originated from adsorbed molecules in different environments. The assignment of the peak at 3697 cm^{-1} was not straightforward. Some researchers attributed it to AlOH, while others considered it due to incomplete dehydration [3,16]. Ward studied the water adsorption on calcium Y zeolite and found a similar peak at 3585 and 3640 cm^{-1} that originated from adsorbed water [16]. He found that the chemisorption of pyridine did not affect the 3585 cm^{-1} band but decreased the 3640 cm^{-1} band to one-eighth of its original intensity. These observations suggest that the band at 3573 cm^{-1} in Fig. 2 represents nonacidic hydroxyl groups, while those associated with the 3636 cm^{-1} band are acidic, like the hydroxyl groups of HX zeolite. The band at 3636 cm^{-1} was very weak, indicating that hydrated CsX has very weak or almost no acidity. The dark, thermal oxidation of 1-butene on CaY and SrY was studied by Tang et al. [2]. They also observed the formation of water during the oxidation reaction, which agrees well with our results.

Fig. 3 shows the FT-IR spectra of NaX exposed to dioxygen and 1-butene, dioxygen and butane, 1-butene, butane, and dioxygen respectively after being pretreated at 773 K, then evacuated at 10^{-4} Torr for 30 min at 473 K. Similar to CsX, bands at 1686, 1588, 1433, and 1377 cm^{-1} were observed when 1-butene and dioxygen were co-fed. As discussed earlier, carboxylate bands in zeolite Y are found at 1584 and 1367 cm^{-1} [14]. Moreover, the band associated with the C=O of acetone is SrY is observed at 1682 cm^{-1} [14]. Since the adsorption of CO_2 in NaX gives true carbonate bands at 1484 and 1430 cm^{-1} [11], the bands in Fig. 3(a) and (b) are most likely due to partial oxidation products. Whereas the features in Fig. 1 (CsX) are due to surface carbonates and/or partial oxidation products, the peaks in Fig. 3 (NaX) are attributed to partial oxidation products only. The FT-IR spectra of butane and dioxygen adsorption on NaX showed no apparent IR bands. Interestingly, a small band at 1622 cm^{-1} was detected in spectrum (c) in Fig. 3 after 1-butene adsorption at 473 K. This feature was attributed to the symmetric stretching of the C=C of the adsorbed 1-butene, suggesting that a small amount of 1-butene adsorbed on NaX at 473 K. Marra et al. studied the CO adsorption on different zeolites [17]. They found a strong correlation between the sorbate–zeolite interaction and the electrical field strength. They reported the local electric field of Na^+ in NaY and Rb^+ in RbNaY to be 5.10 and 2.39 V nm^{-1}, respectively [17]. Therefore, the different IR spectra of butene adsorption on CsX and NaX were probably the result of electrostatic fields in the zeolites with different cations (ionic radii R_{Na^+} = 0.99 Å, R_{Cs^+} = 1.83 Å).

In the range of the hydroxyl stretch, several bands at 3574, 3635 and 3697 cm^{-1} were present after 1-butene oxidation. The bands present in the 3000–4000 cm^{-1} region are always accompanied by the water bending band at 1640 cm^{-1} [16]. However, in our experiment, this band at 1640 cm^{-1} was probably obscured by other peaks at 1595, 1616 and 1686 cm^{-1}. In spectrum (c) of Fig. 4, the intensity of the band at 3635 cm^{-1} was stronger than that of the similar peak in Fig. 2 spectrum (c).

3.2. Catalytic oxidation of 1-butene and butane over zeolites

Fig. 5 presents the reaction profile during butene oxidation in a fixed bed reactor at 473 K on ion-exchanged CsX. The production rate of CO_2 was very low during the initial 200 min although the consumption of O_2 was significant. However, after

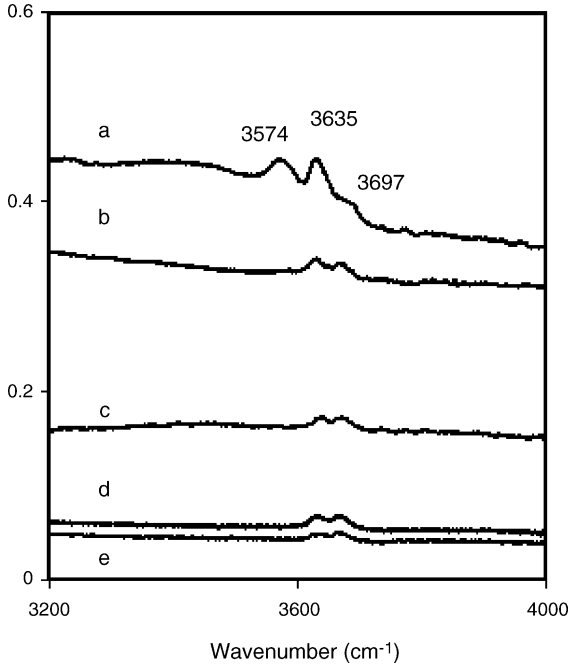

Fig. 4. Infrared spectra of the hydroxyl region of NaX at 473 K. The individual spectra are associated with pretreatments designated in Fig. 3.

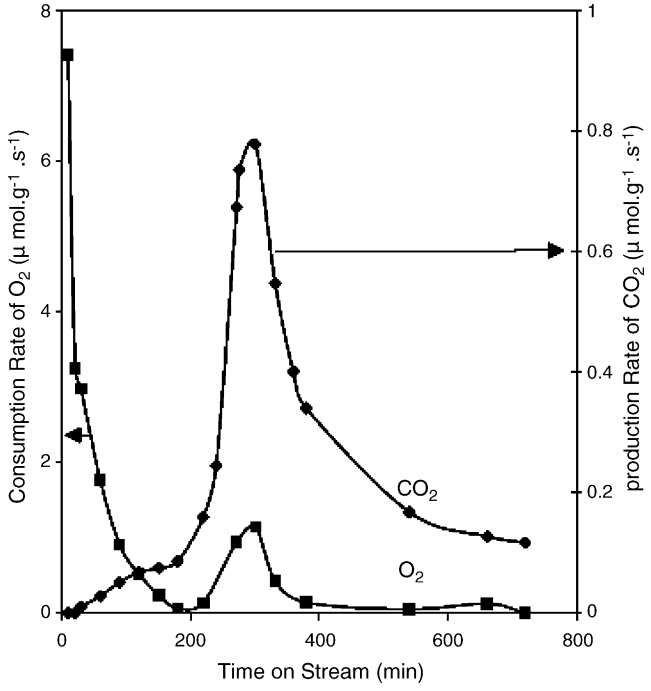

Fig. 5. Butene oxidation over CsX in a fixed bed reactor at 473 K. Total flow rate = 43 mL min^{-1}; He:O_2:butene = 9:1:1.

continued exposure to 1-butene and dioxygen, the activity for CO_2 production increased rapidly over a period of 100 min to a maximum and then decreased rapidly. Unidentified heavier products were observed after 250 min on stream. The double-bond isomerization of 1-butene was observed during the initial 10 min, and then decreased very quickly to zero. The cis/trans ratio was about 9, which suggests that the CsX was base catalyst and the CO_2 formed during the butene oxidation poisoned the few butene isomerization sites on CsX. The CO_2 poisoning experiment in our previous work showed that the basic sites desorbing CO_2 below 473 K have no activity in butene isomerization, which is consistent with our current results [18]. The initial uptake of O_2 at short time on stream is likely being used to partially oxidize the hydrocarbon until CO_2 is eventually produced. Evidence of partial oxidation from IR spectroscopy supports this idea. During the reaction time on stream from 200 to 300 min, the consumption rate of dioxygen and production rate of CO_2 were about the same within the detection limit. From 300 to 500 min, the O_2 consumption rate is lower than the production rate of CO_2. Interestingly, small amounts of heavy products were still observed during this period probably because of the release of previously formed intermediates or products.

In a typical catalytic reaction, the reaction rate is the highest at the beginning, followed by deactivation with time on stream. However, for butene oxidation on zeolite, the production rate of CO_2 was very low during the first 200 min. The complicated behavior of this reaction is not yet completely understood. One possibility is that the adsorption of CO_2 on the zeolite resulted in a low CO_2 effluent concentration. If we assume the reaction rate begins with the maximum rate of 0.8 μmol s^{-1} g^{-1} (the rate at the peak maximum in Fig. 5) then the total amount of CO_2 uptake by the CsX should be 11,029 μmol g^{-1}, which is significantly higher than the CO_2 adsorption capacity of CsX at 373 K (9.6 μmol g^{-1}) [18]. This large difference suggests that the CO_2 adsorption on CsX cannot explain the low initial CO_2 production rate.

Another possibility is that the butene oxidation on CsX proceeds by a free radical chain mechanism. Usually an addition of excess initiator is needed to activate the free-radical chain reaction, but the reaction can be self-activated by mild thermal conditions due to the strong electrical field of the zeolite structure [1,17]. Researchers have demonstrated that alkali and alkaline earth exchanged zeolite Y selectively oxidizes alkanes at low temperature [1,6,8,19]. The reaction mechanism proposed by Frei and coworkers involved a charge-transfer complex $RH^+O_2^-$ [6]. The charge-transfer complex can split further to $R^\bullet$ and $HOO^\bullet$, which act as initiators for the free radical chain reaction. Scheme 1 presents the general pathway for free-radical chain oxidation [20]. The initial low activity for CO_2 production in Fig. 5 may be explained by the induction time required for the production of enough free radicals to propagate the reaction.

Another explanation for the induction time to produce CO_2 is the build up of partial oxidation products in the zeolite pores that eventually react to form CO_2. This explanation is quite probable given the evidence of partial oxidation products observed by IR spectroscopy. Moreover, others have observed

Initiation:

$$In_2 \xrightarrow[k_{I,1}]{} 2In^\bullet$$

$$In^\bullet + RH \rightarrow InH + R^\bullet$$

$$ROOH \xrightarrow[k_{I,2}]{} RO^\bullet + {}^\bullet OH$$

$$RO^\bullet + RH \longrightarrow ROH + R$$

$${}^\bullet OH + RH \longrightarrow HOH + R$$

Propagation:

$$R + O_2 \longrightarrow ROO^\bullet$$

$$ROO^\bullet + RH \xrightarrow[k_P]{} ROOH + R^\bullet$$

Termination:

$$2ROO^\bullet \xrightarrow[k_T]{} NRP + O_2$$

Scheme 1. General pathway in free radical chain oxidation [20]. In = initiator; NRP = non-radical products.

partial oxidation of hydrocarbons in zeolites at low temperature [14]. It is quite interesting that CO is not observed in our study.

Fig. 6 reports the O_2 consumption rate as well as the CO_2 production rate during 1-butene oxidation over CsX in a fixed bed reactor at 523 K. The production rate at 523 K reached a maximum of 2.6 μmol g^{-1} s^{-1} at 160 min in Fig. 6, while the production rate at 473 K reached a maximum of 0.8 μmol g^{-1} s^{-1} at 300 min (Fig. 5). Therefore, the time period required for the CO_2 reaction to reach maximum at higher temperature was much shorter than that at lower temperature. Double-bond isomerization of 1-butene was also observed at 523 K, and then decreased very quickly to zero. A broad peak from the chromatograph was also observed. The retention time of this peak was the same as the one observed at 473 K, suggesting that similar heavy products were produced in the partial oxidation of 1-butene over CsX at 523 K. Similar

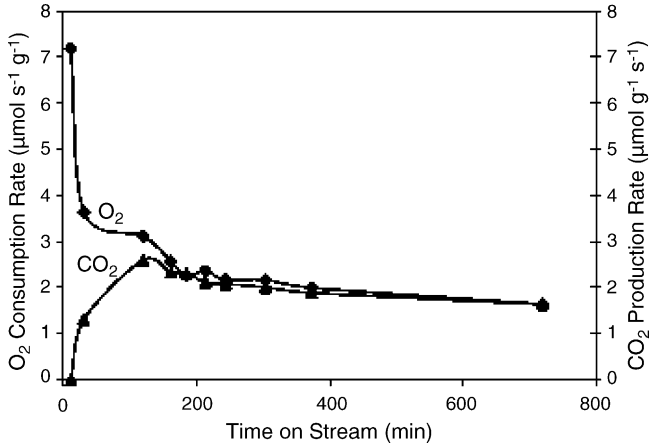

Fig. 6. Butene oxidation over CsX in a fixed bed reactor at 523 K. Total flow rate = 43 mL min^{-1}; He:O_2:butene = 9:1:1.

trends were found during butane oxidation over ion-exchanged zeolite X, except that the overall rates were lower.

Table 1 summarizes the observed maximum reaction rate of butene and butane oxidation on different catalysts in the temperature range from 473 to 523 K. The butane oxidation rate on CsX and NaX was much lower than that of butene oxidation. This result is consistent with the lower ionization potentials and C–H bond energies of alkenes compared to those of alkanes. The Cs-loaded zeolite X possessed activity for butene oxidation although the oxidation rate was lower than that of ion-exchanged CsX, which further proves that the ion-exchanged zeolite was responsible for the oxidation activity instead of the occluded alkali metal compound. Those results were consistent with the in situ FT-IR spectroscopy of butene oxidation on zeolites. The lower activity of Cs/CsX (14 excess Cs atoms per unit cell) was probably due to the occlusion of excess Cs species, which might change the electric field of the cations associated with the framework or block access of the sorbates to the cations. Both CsX and NaX exhibited higher activity for butene oxidation compared to non-zeolite catalysts. Silica gel and γ-Al_2O_3 showed no activity in butane oxidation and very low activity in butene oxidation, indicating the zeolite structure plays an important role in the thermal hydrocarbon oxidation. The MgO and Cs/γ-Al_2O_3 samples also revealed very low activity for butene oxidation, which demonstrates that basicity is not the key feature for oxidation.

The butene oxidation rate on MgY shown in Table 1 was much lower than that of NaX and CsX. Blatter et al. have found that the alkaline earth zeolite Y enhanced thermal propane oxidation at 423 K but did not exhibit thermal oxidation activity of unsaturated hydrocarbons such as low olefins or toluene [6]. They attributed this phenomenon to the strong interaction of olefins and toluene with exchanged cations in the supercage. Therefore, the low activity of MgY might be the result of the strong interaction of butene with Mg^{2+} in the zeolite supercage. Bandyopadhyay and Yashonath found that sorbate–zeolite interactions have a profound influence on the mobility of the sorbates [21]. However, a more plausible explanation for the low activity of MgY can be found in the recent work of Xu et al. [14]. They conclude that both shielding of the small Mg^{2+} cations by oxygen atoms of the zeolite as well as the presence $Mg(OH)_x$ in the pores reduce the ability of MgY to effectively catalyze oxidation reactions.

Elemental analysis performed by Galbraith Lab. (Knoxville, TN) gave the Fe level in the commercial NaX as 102 ppm. It is well known that Fe(III) could act as an oxidizer and reduce to Fe(II) in a redox cycle [22]. Due to the existence of a trace amount of Fe in the zeolite, the contribution of Fe to the activity of hydrocarbon oxidation cannot be totally excluded.

Table 1
Maximum rates of butene and butane oxidation over zeolites, magnesia, silica and alumina

Catalyst	Temperature (K)	Production rate of CO_2[a] (μmol g^{-1} s^{-1})	
		1-Butene oxidation	Butane oxidation
CsX	473	0.80	0.13
	523	2.6	–
NaX	473	0.85	0
	523	5.3	0.093
MgY	473	0.075	–
	523	–	0.14
MgO	473	0	0
	523	0.01	0
Cs/CsX (14)[b]	473	0.19	–
Cs/γ-Al_2O_3 (23 wt.%)	473	0	0
	523	0.0033	0
Silica gel	523	0.0021	0
γ-Al_2O_3	523	0.0035	0

[a] The production rate of CO_2 is based on the maximum reaction rate measured in a fixed bed reactor; total flow rate = 43 mL min^{-1}, He:O_2:butene (butane) = 9:1:1

[b] The sample contains 14 excess cesium atoms/unit cell of zeolite.

3.3. Zeolite-catalyzed condensation of propionic acid and formaldehyde

The effectiveness of alkali-exchanged zeolite X, with and without occluded alkali metal compounds, for the base-catalyzed aldol condensation of propionic acid (PA) with formaldehyde (FA) to methacrylic acid (MAA) was also investigated. Bailey et al. suggested a possible reaction network as shown in Scheme 2 [23]. The major side reactions involve conversion of PA to 3-pentanone (3-P) and subsequent reaction of MAA to heavier products. We explored the possibility of using zeolite base catalysts to prevent the formation of heavy side products.

A summary of the conversion and selectivity from the condensation reaction is reported in Table 2. The conversion was directly correlated to the expected basic strength of the alkali-exchanged zeolites (NaX < KX < CsX). The impregnated catalyst 12% Cs/CsX exhibited even higher activity. This result is not surprising, since previous studies have shown that activity correlates with basic strength [23]. Twelve weight percent of cesium on CsX corresponds to about 16 Cs atoms per unit cell, or 2 Cs atoms per supercage.

The aldol condensation reaction was also carried out over various loadings of cesium-loaded silica (doped with Bi) Cs/Bi/

Table 2
Conversion of PA and selectivity to MAA over basic zeolites[a]

Catalyst	Surface area (m^2 g^{-1})	X_{PA}[b] (%)	S_{MAA}[c] (%)
NaX	596	0.1	~100
KX	–	0.3	~100
CsX	373	0.8	~100
6% Cs/CsX	–	0.8	~100
12% Cs/CsX	197	4.1	82

[a] Reaction was performed at 598 K at catalyst loading of 0.05 g. Feed ratio of PA:FA = 3:2. Liquid reactants fed to the reactor at a rate of 0.4 mL h^{-1}, mixed with a helium stream at 35 mL min^{-1}. Conversion and selectivity reported after 100 min on stream.

[b] Conversion of propionic acid.

[c] Selectivity to methacrylic acid.

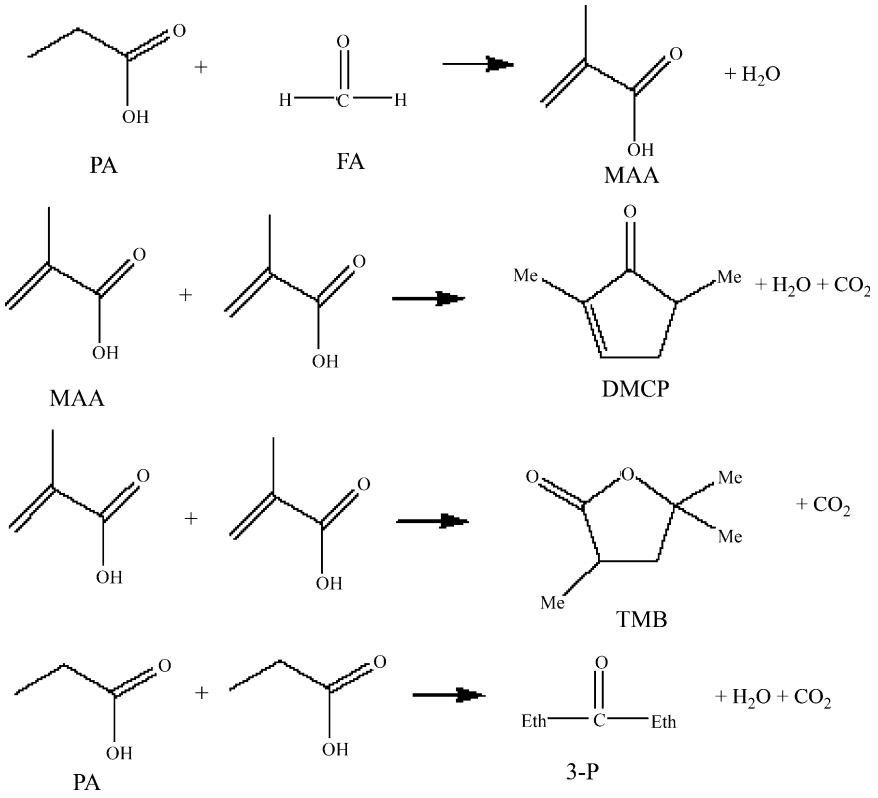

Scheme 2. Suggested reaction network of aldol condensation of propionic acid with formaldehyde. PA: propionic acid; FA: formaldehyde: MAA: methacrylic acid; 3-P: 3-pentanone; DMCP: 2,5-dimethyl-2-cyclopenten-l-one; TMB: 2,4,4-trimethylbutyrolactone.

SiO_2 and cesium-loaded zeolite 12% Cs/CsX in the reactor (Fig. 7). Although silica is not active for the condensation reaction, addition of cesium forms an effective catalyst [23]. Moreover, promotion of an active Cs/silica catalyst with bismuth has been reported in the literature [24]. In our work, the conversion of PA was roughly three times higher on Cs/Bi/SiO_2 than on 12% Cs/CsX at high loading, indicating that a non-zeolitic catalyst is better for this reaction. Presumably, heavy products were formed in the zeolite micropores that block access to the active sites. At a loading of 0.05 g, the turnover frequency (TOF) was calculated to be 0.0054 s^{-1} for Cs/Bi/SiO_2, and 0.0011 s^{-1} for 12% Cs/CsX based on the nominal cesium loading added by impregnation. Evidently, the cesium was more effectively utilized on the silica support. The conversion of PA is clearly non-linear with the catalyst loading.

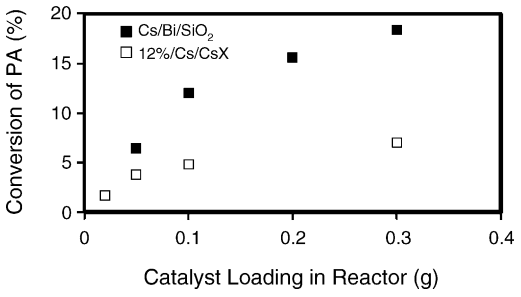

Fig. 7. Effect of loading of catalyst on the conversion of PA over Cs/Bi/SiO_2 and 12% Cs/CsX. Reaction was performed at 598 K. Results are reported after 100 min on stream.

The conversion of PA increases linearly with catalyst loading up to 0.10 g for Cs/Bi/SiO_2 and up to 0.05 g for 12% Cs/CsX. For Cs/Bi/SiO_2, the selectivity to MAA was not affected by the conversion level (i.e. different catalyst loading). It is interesting to observe that the selectivity to MAA for 12% Cs/CsX is strongly influenced by the conversion level. Lower loadings of catalysts resulted in poor selectivity (∼70–80% selectivity to MAA, with 3-P being the major side product). An increase in the loading of Cs/CsX into the reactor increases both conversion of PA and selectivity to MAA up to a certain level (∼5% of conversion and 85% of selectivity to MAA). However, some heavier product DMCP was observed at 5% conversion of PA. As shown in Scheme 2, two PA molecules react to form 3-P and two MAA molecules react to form DMCP. Therefore, a lower loading of 12% Cs/CsX favors the self-combination of PA and a higher loading favors the condensation reaction. Eventually, higher conversion of PA to MAA leads to the sequential reaction of MAA to form DMCP. In this case, the zeolite X did not act as a shape selective catalyst to prevent further reaction of the product MAA. Wierzchowski and Zatorski studied the reaction of methyl propionate with formaldehyde to form methyl methacrylate over a variety of zeolites [25]. They reported that the best conversion and selectivity were observed over a potassium-exchanged Y zeolite that had been treated with potassium hydroxide. Since residual acidity of the zeolite was shown to be detrimental to the selectivity of the reaction, treatment with base was a key step to improve the catalyst. Those observations are consistent with the results reported in this paper.

4. Conclusions

Faujasite-type zeolites containing alkali metal cations are interesting materials that catalyze both oxidation and condensation reactions. Among the ion-exchanged zeolites, those containing Na or Cs had a high reaction rate for butene oxidation compared to a zeolite containing Mg. Addition of Cs to CsX beyond ion-exchange capacity decreased the butene oxidation rate, indicating that the ion-exchanged zeolite was responsible for the oxidation activity. In general, the butane oxidation rate was lower than that of butene oxidation over the zeolites. Furthermore, silica gel, γ-Al_2O_3 and Cs-doped γ-Al_2O_3 were inactive in butane oxidation and minimally active in butene oxidation. Results from these studies suggest that the high electric fields associated with cations inside the micropores of the zeolite are important for the oxidation reaction.

Zeolites were also investigated as catalysts for the condensation of propionic acid with formaldehyde to form methacrylic acid. In this case, the activity was directly related to the basicity of zeolite X, with activity increasing in the series $NaX < KX < CsX$. Moreover, addition of Cs to CsX above ion-exchange capacity increased the condensation rate substantially. However, a zeolite catalyst with occluded Cs was not as effective as a Cs-doped silica catalyst promoted with Bi, presumably because of heavy products blocking the zeolite micropores.

Acknowledgment

This work was supported by the Department of Energy-Basic Energy Sciences (DEFG02-95ER14549).

References

[1] H. Sun, F. Blatter, H. Frei, Catal. Lett. 44 (1997) 247.
[2] S.L.Y. Tang, D.J. McGarvey, V.L. Zholobenko, Phys. Chem. Chem. Phys. 5 (2003) 2699.
[3] J. Xu, B.L. Mojet, J.G. Van Ommen, L. Lefferts, Phys. Chem. Chem. Phys. 5 (2003) 4407.
[4] F. Blatter, F. Moreau, H. Frei, J. Phys. Chem. 98 (1994) 13403.
[5] H. Tsubomura, R.S. Mulliken, J. Am. Chem. Soc. 82 (1960) 5966.
[6] F. Blatter, H. Sun, S. Vasenkov, H. Frei, Catal. Today 41 (1998) 297.
[7] G. Zhang, J.K. Thomas, J. Phys. Chem. B 107 (2003) 7254.
[8] D.L. Vanoppen, D.E. De Vos, P.A. Jacobs, J. Catal. 177 (1998) 22.
[9] W.S. Wieland, R.J. Davis, J.M. Garces, J. Catal. 173 (1998) 490.
[10] J. Li, R.J. Davis, J. Phys. Chem. B 109 (2005) 7146.
[11] E.J. Doskocil, S.V. Bordawekar, B.J. Kaye, R.J. Davis, J. Phys. Chem. B 103 (1999) 6277.
[12] F. Yagi, H. Hattori, Microporous Mater. 9 (1997) 247.
[13] J.W. Ward, H.W. Habgood, J. Phys. Chem. 70 (4) (1966) 1178.
[14] J. Xu, B.L. Mojet, J.G. Van Ommen, L. Lefferts, J. Phys. Chem. B 109 (2005) 18361.
[15] I.A. Beta, H. Boehlig, B. Hunger, Phys. Chem. Chem. Phys. 6 (1975).
[16] J.W. Ward, J. Phys. Chem. 72 (1968) 4211.
[17] G.L. Marra, A.N. Fitch, A. Zecchina, G. Ricchiardi, M. Salvalgaggio, S. Bordiga, C. Lamberti, J. Phys. Chem. B 101 (1997) 10653.
[18] J. Li, R.J. Davis, Appl. Catal. A: Gen. 239 (2003) 59.
[19] J. Xu, B.L. Mojet, J.G. Van Ommen, L. Lefferts, J. Phys. Chem. B 108 (2004) 218.
[20] D.L. Vanoppen, P.A. Jacobs, Catal. Today 49 (1999) 177.
[21] A. Bandyopadhyay, S. Yashonath, Chem. Phys. Lett. 223 (1994) 363.
[22] A. Szegedi, G. Pal-Borbely, K. Lazar, React. Kinet. Catal. Lett. 74 (2001) 277.
[23] O.H. Bailey, R.A. Montag, J.S. Yoo, Appl. Catal. A: Gen. 88 (1992) 163.
[24] J.S. Yoo, Appl. Catal. A: Gen. 102 (1993) 215.
[25] P.T. Wierzchowski, L.W. Zatorski, Catal. Lett. 9 (1991) 411.